


Gold@Mesoporous Polydopamine Nanocomposite Hydrogel Loaded with Estrogen for the Treatment of Skin Photoaging

Dashuai Li¹, Yonghua Wang², Wanyi Zhao³, Liqun Li³, Pan Zhang³ 

¹Department of Stomatology, The First Affiliated Hospital of Wenzhou Medical University, Wenzhou, Zhejiang, 325000, People's Republic of China;

²Department of Ophthalmology, The First Affiliated Hospital of Wenzhou Medical University, Wenzhou, Zhejiang, 325000, People's Republic of China;

³Department of Plastic Surgery, The First Affiliated Hospital of Wenzhou Medical University, Wenzhou, Zhejiang, 325000, People's Republic of China

Correspondence: Pan Zhang, Email 15257752896@163.com

Introduction: Topical application of 17 β -estradiol (E2) has been shown to improve various hallmark features of skin aging, including enhancing skin elasticity and hydration, reducing wrinkles, and promoting collagen synthesis. However, the role of estrogen in UVB-induced photoaging of the skin remains unclear. Furthermore, E2's clinical application is limited by issues such as bioavailability and potential adverse effects. Therefore, this study aims to explore the role of E2 in UVB-induced skin photoaging and to prepare a gold (Au)@mesoporous polydopamine (mPDA)-hyaluronic acid (HA)/carboxymethyl chitosan (CMCS) nanoparticle composite hydrogel (Au/E2@mPDA-HCG) for the treatment of skin photoaging.

Methods: This study successfully fabricated mPDA with a well-defined mesoporous structure and incorporated Au NPs into the mesopores of mPDA using an in situ growth method, thereby constructing Au@mPDA NPs loaded with E2. Subsequently, the Au/E2@mPDA NPs were embedded into a HA/CMCS hydrogel to develop the Au/E2@mPDA-HCG nanoparticle composite hydrogel. The composite hydrogel was characterized through in vitro and in vivo experiments, and its efficacy in improving skin photoaging was evaluated.

Results: This study revealed that estrogen deficiency significantly exacerbates UVB-induced skin photoaging, likely through mechanisms closely associated with increased oxidative stress and reduced collagen production. Moreover, the Au/E2@mPDA-HCG nanoparticle composite hydrogel demonstrated favorable morphological characteristics and biocompatibility. In vitro and in vivo experimental results indicated that this composite hydrogel effectively enhanced the therapeutic efficacy of E2 in treating skin photoaging, as evidenced by its significant mitigation of oxidative stress and inflammatory responses, along with the promotion of collagen synthesis.

Conclusion: In conclusion, this study suggests that the combination of E2 with Au@mPDA@HCG nanocomposite hydrogel offers a promising therapeutic strategy for UVB-induced skin photoaging.

Keywords: estrogen, skin photoaging, Au nanoparticle, mesoporous polydopamine, hyaluronic acid /carboxymethyl chitosan hydrogel

Introduction

The skin is the largest organ of the human body¹ and serves as the primary barrier against external insults. However, it is highly susceptible to damage and aging due to ultraviolet (UV) radiation, environmental pollutants, and extreme temperatures.² Among these factors, UV exposure is a major contributor to skin aging, and the aging process specifically induced by UV radiation is referred to as photoaging.³ Clinically, photoaging manifests as dryness, desquamation, thickening, loss of elasticity, and uneven pigmentation. It is also frequently associated with skin conditions such as acne, seborrheic keratosis, pigmentation disorders, and even skin tumors.⁴ Studies have shown that among the different UV wavelengths, UVB (280–320 nm), despite comprising only 4%–5% of total solar radiation, is the primary cause of skin damage.⁵ Prolonged exposure to UVB leads to excessive accumulation of reactive oxygen species (ROS), DNA damage,

inflammation, and disruption of skin barrier function, ultimately contributing to skin aging and even skin cancer.⁶ The detrimental effects of UVB-induced photoaging not only impose psychological and social burdens on affected individuals but also pose significant public health concerns, particularly in relation to UV-induced skin malignancies.⁷ Although sunscreens and skincare products provide some level of UV protection, their efficacy in reversing photoaging remains limited. Moreover, existing therapeutic agents, including retinoic acid, 5-fluorouracil, and antioxidants, are often associated with adverse effects and application restrictions.⁷ Therefore, there is an urgent need to develop safe and effective therapeutic strategies to mitigate UVB-induced photoaging.

Human epidermal keratinocytes and fibroblasts express estrogen receptors ER α and ER β , whose natural ligand, estrogen, plays a crucial role in skin physiology.⁸ Estrogens are a group of steroid hormones comprising four major forms: estrone, 17 β -estradiol (E2), estriol, and estetrol, with E2 mediating most of their biological effects.⁹ Studies have shown that estrogens can mitigate skin aging and wrinkle formation, enhance skin thickness, increase dermal collagen content and water retention capacity, improve epidermal barrier function, and maintain skin hydration.⁸ Additionally, phytoestrogens exhibit anti-aging properties by preventing oxidative damage and restoring skin hydration and collagen levels.¹⁰ These findings suggest that estrogens hold potential as therapeutic agents for skin anti-aging. However, as pleiotropic hormones, the effects of estrogens *in vivo* are significantly influenced by their route of administration.¹¹ When administered orally, the majority of E2 is metabolized in the liver into estrone (E1), which possesses only one-tenth of the biological activity of E2. Furthermore, supraphysiological estrogen levels in the liver may increase the risk of thrombosis and suppress growth hormone-mediated insulin-like growth factor 1 (IGF-1) production.¹² On the other hand, injectable estrogen undergoes hepatic metabolism upon entering the liver via the portal vein, leading to a substantial reduction in the bioavailable estrogen concentration in the skin, thereby limiting its therapeutic efficacy. Consequently, enhancing the bioavailability of estrogens while minimizing their adverse effects has become a key focus of current research.

With the rapid advancement of materials science and nanotechnology, nanocarrier-mediated delivery systems have opened new possibilities for cutaneous drug delivery systems, enhancing both efficacy and safety.¹³ Among various nanocarriers, gold nanoparticles (AuNPs) have emerged as a research hotspot in the field of transdermal drug delivery due to their excellent biocompatibility, tunable particle size, surface chemistry, and unique plasmonic properties.¹⁴ Studies have shown that AuNPs exhibit anti-inflammatory and immunomodulatory effects, demonstrating potential applications in the treatment of various skin diseases.¹⁵ However, AuNPs tend to aggregate, leading to decreased performance and stability.¹⁶ Therefore, surface modifications are necessary to enhance their biocompatibility and stability.^{17,18} Recently, mesoporous polydopamine (mPDA) nanoparticles with systematically tailored pore structures have attracted significant attention in drug delivery applications. Their well-defined mesoporous architecture enables efficient drug encapsulation, thereby substantially improving drug delivery efficiency.¹⁹ Moreover, mPDA exhibits exceptional metal chelation capabilities, serving as an ion anchor for various metal ions, including Mn⁺ and Au⁺.²⁰ Zhou et al demonstrated that coating AuNPs with mPDA significantly enhances their stability, while the mesoporous structure facilitates drug loading, ultimately improving therapeutic efficacy.²¹

The efficacy of drug delivery systems is closely related to the route of administration.¹⁷ Previous studies have shown that estrogen exhibits significantly reduced bioavailability and may induce systemic side effects when administered orally or via injection.¹² Therefore, in addition to utilizing drug carriers to enhance estrogen bioavailability, it is crucial to explore an administration method that effectively minimizes systemic adverse effects. In recent years, transdermal drug delivery has gained considerable attention due to its advantages, including ease of application, avoidance of first-pass hepatic metabolism and gastrointestinal disturbances, and controlled drug release.²² Among transdermal drug delivery systems, hydrogels have been extensively studied for the treatment of photoaging due to their high water content, biocompatibility, biodegradability, and drug release modulation capabilities.^{23,24} Both natural and synthetic polymers can be used for hydrogel fabrication. Among them, hyaluronic acid (HA) and carboxymethyl chitosan (CMCS) have been widely applied in drug-controlled release and tissue engineering due to their excellent biocompatibility and biodegradability.²⁵ HA plays a crucial role in skin hydration, delaying skin aging, and promoting wound healing.²⁶ However, it cannot form a hydrogel structure independently, necessitating the design of HA-based hydrogel formulations.²³ Meanwhile, CMCS exhibits antioxidant activity and promotes fibroblast proliferation, making it

a valuable component in skin improvement strategies.²⁷ CMCS is often combined with other polymers to fabricate hydrogels with superior biocompatibility and moisturizing properties, which have been widely applied in medical and healthcare-related fields.²⁸ Studies have shown that HA/CMCS composite hydrogels encapsulating therapeutic agents have been explored for skin anti-aging applications,²⁹ offering a promising strategy for the development of efficient and low-adverse-effect estrogen delivery systems.

Based on this, the present study first investigated the effects of estrogen on UVB-induced skin photoaging in mice through *in vivo* experiments. Subsequently, mPDA with a clear mesoporous structure was successfully prepared, and Au NPs were loaded into the mesopores of mPDA through an *in situ* growth method, forming Au@mPDA NPs and loading them with E2. The Au/E2@mPDA nanoparticles were then incorporated into an HA/CMCS hydrogel to prepare the Au/E2@mPDA-HCG nanoparticle composite hydrogel. The composite hydrogel was characterized through both *in vivo* and *in vitro* experiments, and its ability to improve skin photoaging was evaluated. The results indicated that estrogen deficiency exacerbated the degree of UV-induced skin photoaging in mice. Furthermore, the Au/E2@mPDA-HCG nanoparticle composite hydrogel was successfully prepared, exhibiting excellent morphological structure and physico-chemical properties, and it significantly improved skin photoaging. This study provides important experimental evidence and new insights for developing a photoaging treatment strategy based on nanomaterials and hydrogels.

Materials and Methods

Experimental Animals

Six-week-old female C57BL/6J mice were purchased from SiPeiFu Company (Beijing, China) and housed under appropriate temperature and humidity conditions with free access to food and water, maintaining a 12 h light/dark cycle. All animal experimental protocols were conducted in accordance with the guidelines of the National Institutes of Health for the care and use of laboratory animals and the ARRIVE guidelines. The research protocol was approved by the Laboratory Animal Ethics Committee of Wenzhou Medical University (approval number: wyd2024-0556).

Grouping and Treatment of Mice

Six-week-old female C57BL/6J mice were acclimatized for one week before exposure to UVB and undergoing bilateral ovariectomy (OVX) surgery. The mice were randomly divided into four groups (n=6 per group): Control, UVB, OVX, and UVB+OVX. For the OVX and UVB+OVX groups, estrogen deficiency was induced by OVX surgery. The specific procedure for the OVX surgery was as follows: The mice in the OVX and UVB+OVX groups were anesthetized using isoflurane (induction: 3%, maintenance: 1.5%) and fixed. The fur on both sides of the lower one-third of the back midline was shaved, and the surgery was performed. A 0.5 cm incision was made through the skin and dorsal muscle, revealing a shiny, whitish fat pad containing the ovaries. The fat pad was gently grasped with small forceps and pulled outside the incision. The fat pad was then separated, and the ovarian ligaments were tied with sutures and the ovaries were excised. Afterward, the uterus was returned to the abdominal cavity, and the incision was sutured. The ovaries on the other side were removed using the same method. For the Control and UVB groups, the same surgical procedure was performed, but the ovaries were not removed. One week after the surgery, the mice's back hair was shaved using an electric razor. Subsequently, the backs of the UVB and UVB+OVX groups were exposed to a narrowband UVB light source (wavelength 290–320 nm, peak wavelength 312 nm, TL20 W/12). During the exposure, the mice were placed in a closed activity box and allowed to move freely, with the light source positioned 25 cm above the box. UVB irradiation was administered five times a week for eight weeks. At the end of the experiment, all mice were euthanized, and their back skin tissues and serum samples were collected for further analysis.

Histological Analysis

The mouse skin tissues were fixed in 10% formalin solution, embedded in paraffin, and sectioned into 5 µm thick slices. The sections were then stained with hematoxylin and eosin (H&E, Abcam) according to the standard protocol. To evaluate collagen deposition, skin tissue sections were stained using the Masson trichrome staining kit (Abcam) following the manufacturer's instructions. All images were captured using an optical microscope.

Enzyme-Linked Immunosorbent Assay (ELISA)

The levels of E2 in serum samples, and SOD and MDA in mouse skin tissue and HaCaT cells were detected using an ELISA kit (Thermo Scientific, USA). Briefly, the diluted protein standards and samples were added to the wells of a 96-well ELISA plate. Then, an antibody specific to the biochemical molecule was added. After washing with a washing buffer, an avidin-horseradish peroxidase conjugate solution was added to each well. The reaction was terminated using a stop solution. The optical density (OD) values were measured at 450 nm for E2 and MDA, and at 560 nm for SOD.

Dihydroethidium (DHE) Staining

To prepare paraffin-embedded skin tissue sections (5 μm), in situ ROS detection was performed using DHE staining solution (Thermo Fisher Scientific). Specifically, after deparaffinization and rehydration, the tissue sections were incubated in a humidified chamber at 37°C with DHE solution (10 μM) in the dark for 1 h. Upon interaction with the superoxide anion in the samples, DHE is oxidized, producing bright red fluorescence. The fluorescence was then detected using an Olympus Fluoview FV1000 confocal microscope.

Preparation of Au/E2@mPDA NPs

Preparation of mPDA NPs

Dissolve 0.15 g of dopamine hydrochloride and 0.10 g of Pluronic F-127 in a mixture of water and ethanol (1:1), with a total volume of 10 mL. Then, under stirring conditions, add 0.20 mL of toluene (TMB, 98%), and sonicate for 2 min to form a uniform emulsion. Next, dropwise add 0.375 mL of ammonia solution to the emulsion system and polymerize for 2 h. After the reaction, centrifuge the resulting nanoparticles three times using a mixture of water and ethanol (1:1), then vacuum dry. Finally, disperse the product in anhydrous ethanol to a concentration of 1 mg/mL for further use.

Preparation of E2@mPDA NPs

Add 100 μL of an E2 ethanol solution (1 mg/mL) to the mPDA NPs suspension (1 mg/mL). Stir and react for 12 h, then separate the E2@mPDA NPs by centrifugation. Finally, redisperse the obtained nanoparticles in water for further use.

Preparation of Au/E2@mPDA NPs

Add 200 μL of $\text{HAuCl}_4 \cdot 3\text{H}_2\text{O}$ solution to the 1 mg/mL E2@mPDA NPs aqueous suspension and stir for 2 h. Then, dropwise add 20 μL of 1% sodium citrate solution at 100°C and continue stirring for 10 min to generate Au/E2@mPDA NPs. Afterward, wash the obtained Au/E2@mPDA NPs with ethanol by centrifuging three times and redisperse them in water for future use. Au@mPDA NPs can be prepared using the same method, but without adding E2.

Characterization of Au/E2@mPDA NPs

The structure and morphology of the NPs were characterized using transmission electron microscopy (TEM, FEI Talos F200X, USA). The zeta potential and hydrodynamic size of the NPs were measured using a nanoparticle size analyzer (Zetasizer Nano ZS, UK). The particle size of the synthesized NPs was determined by dynamic light scattering (DLS), and Fourier-transform infrared spectroscopy (FTIR) analysis was performed. X-ray powder diffraction (XRD) spectra were obtained using an X-ray diffractometer. Additionally, to evaluate in vitro stability, mPDA NPs and Au/E2@mPDA NPs were incubated in water and DMEM at 4°C for 30 days, with particle size and PDI measured at designated time intervals.

Preparation and Characterization of Au/E2@mPDA-HCG Nanoparticle Composite Hydrogel

A 1 wt% HA solution and a 3 wt% CMCS solution were prepared in advance. An EDC/NHS solution was added dropwise to the HA solution, and after stirring for 30 min, it was mixed with the CMCS solution in a 1:1 volume ratio. The resulting mixture was rapidly stirred to ensure uniformity and then poured into molds. The mixture was left to stand at 4°C for 12 h to form the HA/CMCS hydrogel (HCG). After gelation, the hydrogel was thoroughly washed

with deionized water to obtain the final HA/CMCS hydrogel. Next, Au@mPDA NPs or Au/E2@mPDA NPs were combined with the CMCS solution to prepare Au@mPDA@HA/HCG and Au/E2@mPDA@HA/HCG hydrogel patches, respectively. Each hydrogel patch contained 100 μg of E2. The microstructure of the hydrogels was observed using scanning electron microscopy (SEM, FlexSEM1000, Japan). Before testing, the samples were freeze-dried and gold-coated.

The in vitro Drug Release of Au/E2@mPDA-HCG Nanoparticle Composite Hydrogel

The release medium used was 1.0% SDS buffer solution. The prepared hydrogel samples were placed in dialysis bags and immersed in 10 mL of release medium within centrifuge tubes. The in vitro release behavior of E2 was assessed under constant shaking at 37°C and 100 rpm. At predetermined time points (1, 2, 4, 8, 12, 24, 36, and 48 h), 1.0 mL samples of the release medium were collected, and an equal volume of fresh release medium was added to maintain the volume. The collected samples were then analyzed using high-performance liquid chromatography (HPLC) to calculate the cumulative release of E2 from Au@mPDA@HA/HCG.

In vitro Transdermal Permeation of Au/E2@mPDA-HCG Nanoparticle Composite Hydrogel

First, ex vivo mouse skin needs to be prepared. Briefly, after anesthetizing the female Balb/c mice, the fur on the back of the mice was shaved using pet clippers, followed by shaving off any remaining short hair with a razor. The mice were then euthanized by cervical dislocation, and the back skin was carefully removed after confirming that there was no damage to the skin. Excess subcutaneous fat, blood vessels, and other tissues were removed, and the skin was placed in a self-sealing bag, sealed, and wrapped in aluminum foil before being stored at -20°C .

After preparing the ex vivo mouse skin, a diffusion cell was used to conduct the in vitro transdermal permeation experiment. A 1.0% SDS buffer solution was selected as the transdermal receptor fluid. The moisture from the prepared mouse skin was absorbed using kitchen paper, and the skin was placed between the donor and receptor chambers. Au/E2@mPDA-HCG was added to the donor chamber, and 10.0 mL of receptor fluid was added to the receptor chamber. At 1, 2, 4, 8, 12, 24, 36, and 48 h, 1.0 mL of receptor fluid was taken from the receptor chamber, and an equal volume of fresh receptor fluid was immediately added. The receptor fluid collected at each time point was analyzed by HPLC, and the cumulative transdermal permeation of E2 from Au/E2@mPDA-HCG was calculated.

In vitro Photoprotective Activity of Au/E2@mPDA-HCG Nanoparticle-Composite Hydrogel

Cell Culture and Treatment

Human keratinocyte cells (HaCaT) were purchased from iCell Bioscience Inc. (Shanghai, China). HaCaT cells were cultured in DMEM medium containing 10% fetal bovine serum and 1% penicillin/streptomycin, and incubated at 37°C, 5% CO_2 , and saturated humidity.

HaCaT cells were randomly divided into the following groups: Control group, UVB group, UVB+E2 group, UVB+Au@mPDA-HCG group, and UVB+Au/E2@mPDA-HCG group. To simulate UVB radiation exposure, HaCaT cells were seeded in 96-well plates at a density of 5×10^3 cells per well. After 48 h of culture, the medium was discarded and the cells were washed twice with PBS. Then, an appropriate amount of PBS was added to each well (enough to cover the cells), and the cells in each group were irradiated using a UV light therapy device. The irradiation conditions were set at an intensity of $0.61 \text{ mW} \cdot \text{cm}^{-2}$ for 5 min. Cells in the Control group were shielded from UV radiation using aluminum foil before exposure. After irradiation, PBS was discarded, fresh medium was added, and the cells were cultured further for subsequent analysis. In the UVB+E2 group, UVB+Au@mPDA-HCG group, and UVB+Au/E2@mPDA-HCG group, the HaCaT cells were treated with E2, Au@mPDA-HCG, and Au/E2@mPDA-HCG, respectively, 24 h before UVB exposure, and the cells were cultured for another 24 h after treatment. The concentration of E2 in the UVB+E2 group and UVB+Au/E2@mPDA-HCG group was $1 \times 10^{-7} \text{ mol/L}$.

CCK-8 Assay

The treated cells (2000 cells per well) were added to 96-well plates, and 10 μ L of CCK-8 solution was added to each well. The cells were incubated at 37°C with 5% CO₂ for 2 h, after which the absorbance at 450 nm was measured to calculate cell viability.

Senescence-Associated Beta-Galactosidase (SA- β -Gal) Staining

According to the manufacturer's instructions, cells were stained using the Senescence β -Galactosidase Staining Kit (Beyotime, China). At room temperature, the culture medium was removed from each group, and the cells were washed once with PBS before being fixed with fixation solution for 15 min. The cells were then washed three times with PBS and incubated with the staining solution at 37°C overnight. The stained cells were observed and photographed using an inverted microscope.

Intracellular ROS Detection

The intracellular ROS levels were measured using the 2', 7'-dichlorodihydrofluorescein diacetate (DCF-DA) method. HaCaT cells were seeded in a 6-well plate and stained with 20 μ M DCF-DA at 37°C for 1 h under dark conditions. After staining, the cells were washed three times with PBS, and fluorescence staining results were observed using a fluorescence microscope (Nikon Eclipse, Tokyo, Japan).

Western Blot Assay

Total protein samples were extracted from HaCaT cells or skin tissue using RIPA lysis buffer. After protein extraction, the protein concentration was determined using a BCA Protein Assay Kit. Equal amounts of protein samples were separated by 10% SDS-PAGE and transferred onto a Polyvinylidene Fluoride (PVDF) membrane. The PVDF membrane was blocked at room temperature for 1 h with 5% skim milk in TBST. Then, primary antibodies (COL I: 1:1000; COL III: 1:1000; NOX1: 1:1000; NOX2: 1:1000; IL-6: 1:1000; β -actin: 1:50000) were added and incubated overnight. After washing the membrane three times with Tris-buffered saline, the PVDF membrane was incubated with the corresponding secondary antibody at room temperature for 30 min. The results were detected using a chemiluminescence imaging and analysis system. All antibodies were purchased from Abcam.

In vivo Photoprotective Activity of Au/E2@mPDA-HCG Nanoparticle-Composite Hydrogel

The method for OVX surgery in mice is described in section 2.2. One week after the OVX surgery, 24 female C57BL/6J mice were divided into four groups: OVX+UVB, OVX+UVB+E2, OVX+UVB+Au@mPDA-HCG, and OVX+UVB+Au/E2@mPDA-HCG, with 6 mice in each group. All mice were shaved on their backs using an electric razor, and their backs were exposed to narrow-band UVB light (wavelength 290–320 nm, peak wavelength 312 nm, TL20 W/12). During the exposure, the mice were allowed to move freely within a closed box. The distance between the light source and the bottom of the box was 25 cm. UVB exposure was administered five times a week for 8 weeks. In addition, one week after the first UVB exposure, the three groups—OVX+UVB+E2, OVX+UVB+Au@mPDA-HCG, and OVX+UVB+Au/E2@mPDA-HCG—received daily topical applications of E2, Au@mPDA-HCG, and Au/E2@mPDA-HCG on their backs, respectively, continuing until the end of the experiment. The dose of E2 in the OVX+UVB+E2 and OVX+UVB+Au/E2@mPDA-HCG groups was equivalent to 5 mg/kg. No treatment was applied to the OVX+UVB group. At the end of the experiment, all mice were euthanized, and their back skin tissue and serum samples were collected for subsequent experimental analysis.

Statistical Analyses

All experiments were repeated at least three times. Data are presented as the mean \pm standard deviation. Statistical analysis was performed using GraphPad Prism 9 (GraphPad Inc, San Diego, CA, USA). One-way analysis of variance (ANOVA) was used for comparisons among multiple groups, followed by Tukey's multiple comparison test. A *P*-value of < 0.05 was considered statistically significant.

Results and Discussion

Estrogen Deficiency Exacerbates Skin Photoaging in Mice

Estrogen prevents skin aging by increasing skin thickness, reducing wrinkles, and enhancing skin hydration. Studies have shown that estrogen treatment can prevent the loss of type I collagen and promote its *de novo* synthesis.³⁰ To investigate the role of estrogen in skin photoaging, we established an OVX mouse model and applied various interventions to examine the impact of estrogen deficiency on skin photoaging. As shown in [Figure 1A](#), compared to the Control group, mice in the UVB, OVX, and OVX+UVB groups exhibited clear skin abnormalities, such as skin damage, redness, and wrinkles, with the most severe skin damage observed in the OVX+UVB group. Considering that increased epidermal thickness and collagen degradation leading to tissue atrophy are characteristic features of skin photoaging,⁶ we performed HE and Masson staining on the dorsal skin of the mice. HE staining results ([Figure 1B](#)) revealed that, compared to the Control group, UVB and OVX groups showed epidermal thickening and dermal thinning. After combined UVB and OVX intervention, epidermal thickening and dermal thinning were more pronounced, along with noticeable epidermal shedding. Furthermore, Masson staining results ([Figure 1B](#)) demonstrated that, compared to the Control group, the collagen content in the dermis of UVB, OVX, and UVB+OVX groups was reduced, with the UVB+OVX group showing the lowest collagen content in the dermis. Additionally, E2 content analysis ([Figure 1C](#)) indicated that serum E2 levels were significantly lower in the UVB, OVX, and OVX+UVB groups compared to the Control group, with the OVX+UVB group exhibiting the lowest E2 levels in the serum. These findings suggest that estrogen deficiency further exacerbates UVB-induced pathological changes in the skin.

Excessive production of ROS is one of the key pathological features of UVB-induced skin photoaging.³¹ The accumulation of ROS exacerbates oxidative stress damage, such as lipid oxidation, which accelerates the aging process of skin cells. One of the major products of lipid oxidation, malondialdehyde (MDA), is commonly used as an indirect marker of oxidative stress.³² Additionally, superoxide dismutase (SOD), as the first line of defense in the skin's antioxidant defense system, catalyzes the dismutation of superoxide anion radicals to produce oxygen and hydrogen peroxide, the latter of which can be further broken down by catalase (CAT) and glutathione peroxidase (GPx).³³ Furthermore, mechanistic studies have shown that ROS can also activate redox-sensitive transcription factor NF- κ B.^{34,35} NF- κ B is a central regulator of the senescence-associated secretory phenotype (SASP) in senescent cells. Activated NF- κ B regulates various pro-inflammatory cytokines, such as IL-6 and TNF- α . IL-6 induces the transcription of matrix metalloproteinase (MMP)-1 in dermal fibroblasts, while TNF- α upregulates the transcriptional expression of MMPs, accelerating the degradation of the extracellular matrix, thereby leading to skin photoaging.³⁶ Studies have shown that OVX effectively decreases serum E2 expression and increases NF- κ B expression.³⁷ Moreover, E2 has been shown to have an inhibitory effect on oxidative stress.⁹ Based on these findings, we further hypothesized that estrogen deficiency may exacerbate skin photoaging. To explore the effects of estrogen on MDA, SOD, and ROS levels during skin photoaging, we conducted MDA and SOD content assays, as well as dihydroethidium (DHE) staining. The results ([Figure 1D–F](#)) showed that, compared to the Control group, MDA and ROS levels were significantly higher, while SOD levels were significantly lower in the UVB, OVX, and UVB+OVX groups, with the UVB+OVX group showing the most pronounced changes. These results suggest that estrogen deficiency significantly aggravates oxidative stress in the skin and reduces collagen synthesis, thereby further promoting the onset of skin photoaging.

Characterization of Au/E2@mPDA NPs

To address the issues of E2 in clinical applications, we designed and synthesized Au/E2@mPDA NPs for E2 delivery. The morphology and structure of mPDA NPs and Au/E2@mPDA NPs were observed using TEM. The results showed ([Figure 2A](#)) that mPDA NPs exhibited a uniform spherical structure with a porous surface, providing favorable spatial conditions for drug loading. After loading Au NPs and E2, the porous structure on the mPDA surface disappeared, indicating successful loading of Au NPs and E2 into the pores of mPDA. Previous studies suggest that changes in zeta potential and particle size can indirectly indicate the successful loading of nanoparticles and drugs.³⁸ Therefore, the particle size of mPDA NPs and Au/E2@mPDA NPs was analyzed in this study. The results ([Figure 2B](#)) showed that the particle size of mPDA was 225.54 ± 5.06 nm, and after loading with

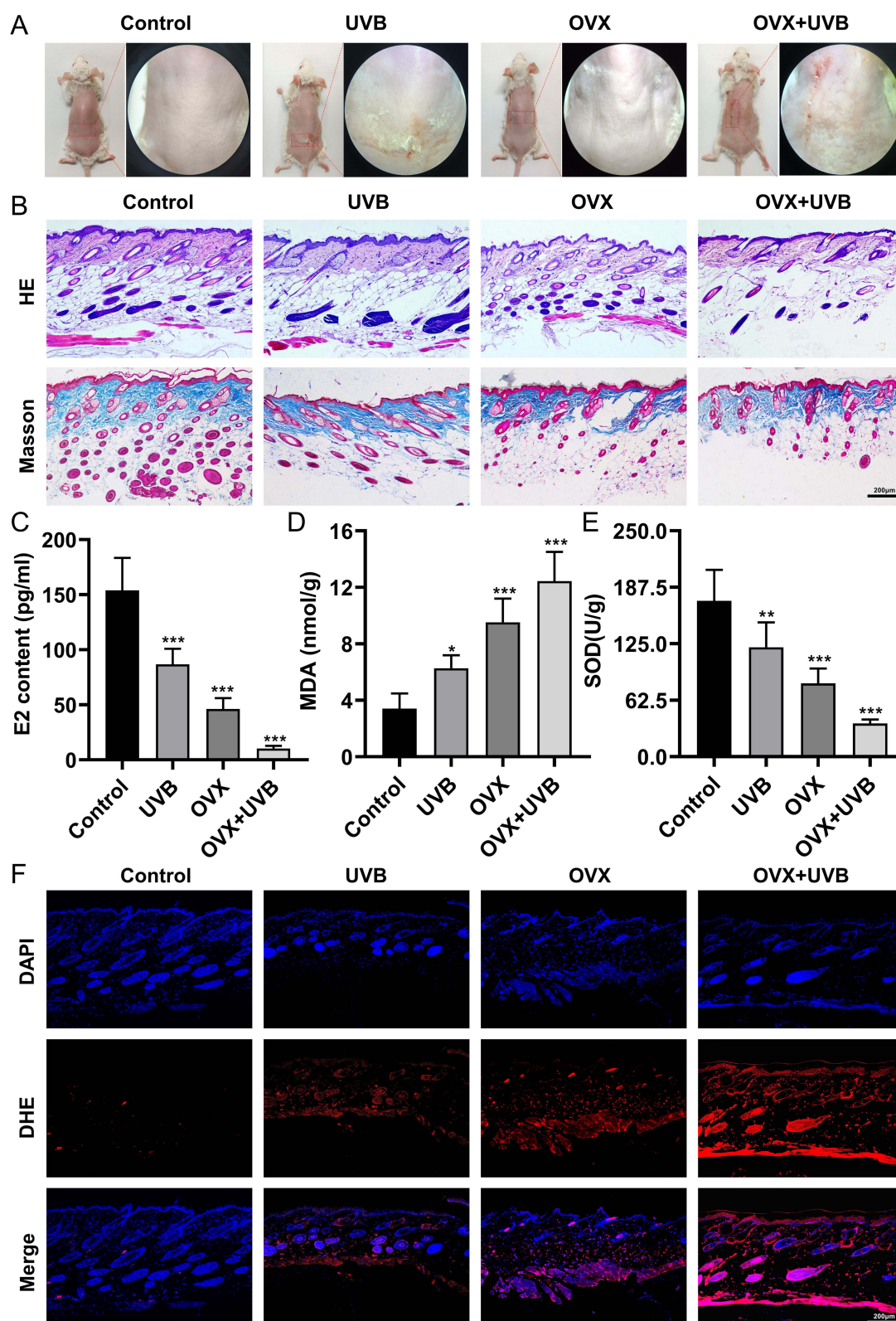


Figure 1 Estrogen deficiency exacerbates skin photoaging in mice. **(A)** Morphological changes of mouse skin after different interventions. **(B)** HE staining (100 \times , $n=3$, top) and Masson staining (100 \times , $n=3$, bottom), bars = 200 μ m. **(C)** ELISA measurement of serum E2 levels in mice ($n=6$). **(D)** ELISA measurement of MDA levels in mouse skin tissue ($n=6$). **(E)** ELISA measurement of SOD levels in mouse skin tissue ($n=6$). **(F)** DHE staining detection of ROS levels in mouse skin (100 \times , $n=3$), bars = 200 μ m. Control, mice without any intervention. UVB, mice exposed to UVB irradiation. OVX, mice subjected to OVX surgery. UVB+OVX, mice exposed to UVB irradiation and subjected to OVX surgery. * $P<0.05$ vs Control, ** $P<0.01$ vs Control, *** $P<0.001$ vs Control.

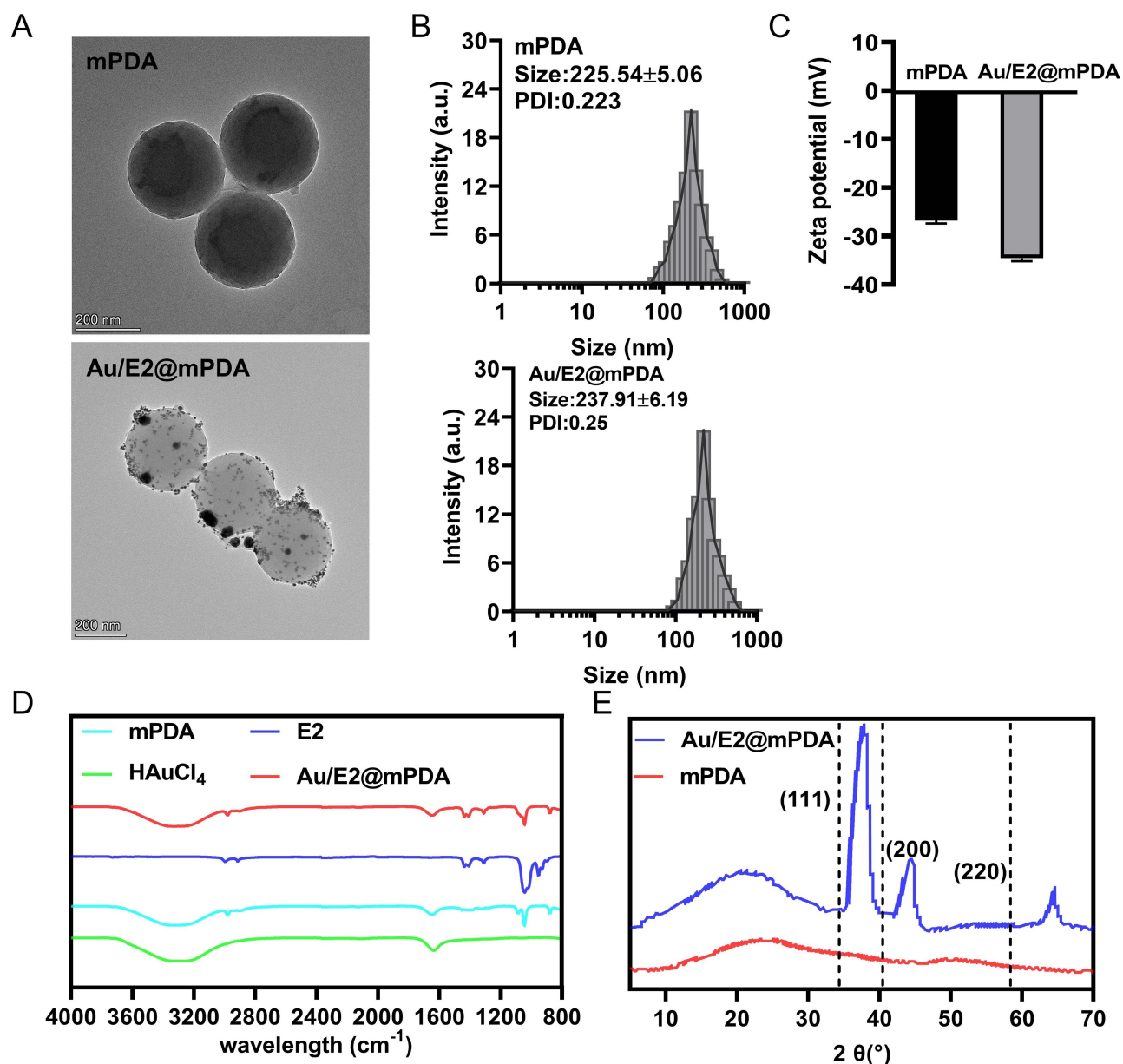


Figure 2 Characterization of Au/E2@mPDA NPs. **(A)** TEM images of mPDA NPs and Au/E2@mPDA NPs, bars = 200 nm. **(B)** DLS analysis of the particle size of mPDA NPs and Au/E2@mPDA NPs. **(C)** Zeta potential of mPDA NPs and Au/E2@mPDA NPs. **(D)** FTIR spectra. **(E)** XRD spectra.

Au NPs and E2, the particle size increased to 237.91 ± 6.19 nm. This is consistent with the reported particle size range (100–300 nm) of mPDA nanomedicines,³⁹ and the increase in particle size may be due to the filling of Au NPs and E2 into the pores of mPDA, leading to an expansion of the particle size. Further zeta potential measurements (Figure 2C) revealed that mPDA NPs, due to their surface rich in hydroxyl groups,⁴⁰ had a zeta potential of approximately - (26.82±0.57) mV. After loading E2 and negatively charged Au NPs,²¹ the negative charge on the nanoparticle surface increased, and the zeta potential decreased to - (34.56±0.61) mV. This change further confirms the successful loading of Au NPs and E2. In addition to particle size and zeta potential analysis, FTIR and XRD analyses were performed to verify the successful incorporation of Au NPs and E2 into mPDA NPs. As shown in Figure 2D, the FTIR results confirmed that Au/E2@mPDA was successfully synthesized, with E2 effectively loaded. The XRD results (Figure 2E) showed characteristic peaks for Au at (111), (200), and (220)

crystal planes, while the original peaks of mPDA were also retained. These findings collectively indicate the successful preparation of Au/E2@mPDA NPs. Moreover, the stability of drug delivery carriers is crucial for their functionality.^{41,42} Thus, this study further evaluated the stability of mPDA NPs and Au/E2@mPDA NPs in water and DMEM medium. The results (Figure 3) showed that both NPs maintained a stable size distribution without significant aggregation or sedimentation after being stored in deionized water or DMEM for 7 or 30 days. These findings indicate that the prepared NPs exhibit good stability, suggesting that Au/E2@mPDA NPs have potential advantages in drug delivery.

Characterization of Au/E2@mPDA-HCG Nanoparticle-Composite Hydrogel

Compared to traditional therapies, hydrogels offer several advantages as local drug delivery systems, including improved patient quality of life, sustained drug release, and drug absorption through the skin barrier.⁴³ In this study, to enhance the transdermal delivery of Au/E2@mPDA NPs, we prepared HA/CMCS (HCG) hydrogel and loaded Au/E2@mPDA NPs into it (Au/E2@mPDA-HCG) for transdermal administration of E2. The macroscopic images of HCG and Au/E2@mPDA-HCG hydrogels are shown in Figure 4A. The mPDA hydrogel is colorless, but upon addition of the brown-black Au/E2@mPDA nanoparticles,³⁹ the color of the hydrogel changes to brown-black. The microstructure of the freeze-dried HCG and Au/E2@mPDA-HCG hydrogels was characterized by SEM analysis. The results (Figure 4B and C) show that the average pore size of HCG hydrogel is 17.15 μm , and after loading Au/E2@mPDA nanoparticles, the pore size decreases to 14.65 μm , indicating the successful loading of Au/E2@mPDA nanoparticles into the HCG hydrogel. Additionally, *in vitro* drug release results for E2 (Figure 4D) show a burst release of free E2, with almost complete release within 12 h, while Au/E2@mPDA-HCG hydrogel released $85.83 \pm 2.11\%$ of the drug within 48 hours and continued to release, demonstrating its sustained-release effect. Further transdermal release analysis of E2 (Figure 4D) revealed that the amount of E2 released transdermally from Au/E2@mPDA-HCG over 48 hours was $57.77 \pm 3.78\%$, indicating that E2 can effectively penetrate the skin to exert therapeutic effects.

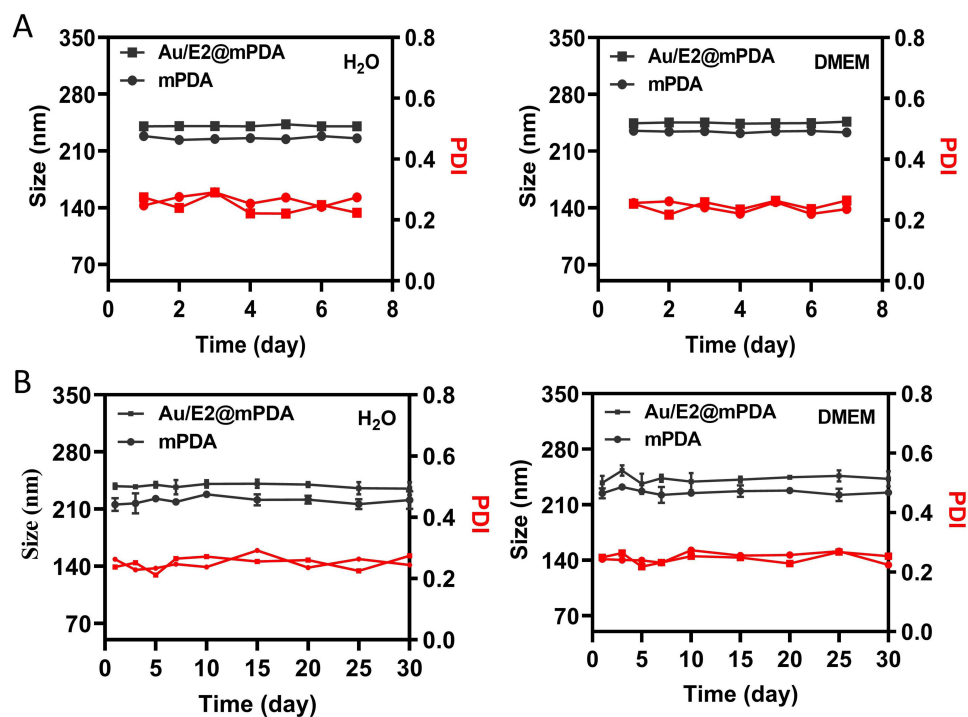


Figure 3 Stability of mPDA NPs and Au/E2@mPDA NPs. (A) Stability study of mPDA NPs and Au/E2@mPDA NPs after incubation in water and DMEM for 7 days. (B) Stability study of mPDA NPs and Au/E2@mPDA NPs after incubation in water and DMEM for 30 days.

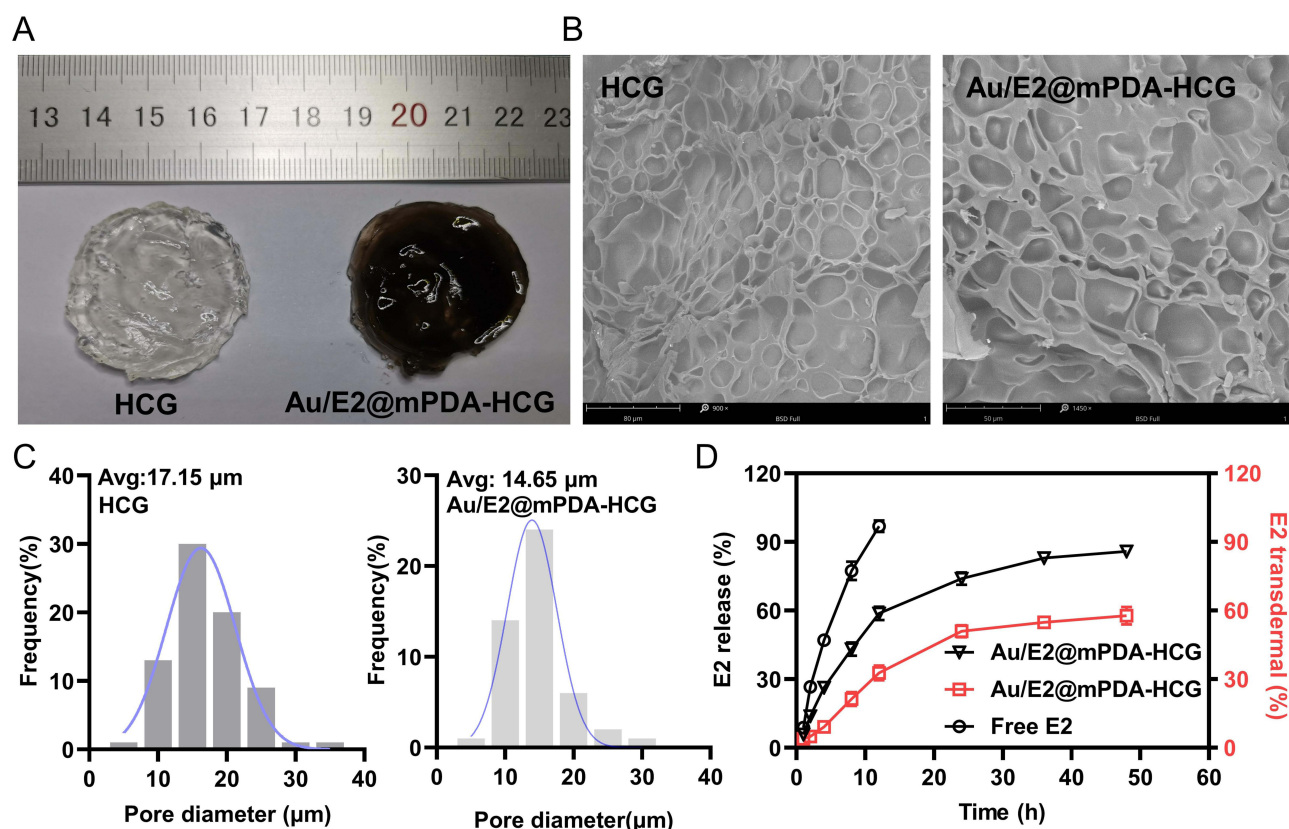


Figure 4 Characterization of Au/E2@mPDA-HCG nanoparticle-composite hydrogel. (A) Macroscopic images of HCG and Au/E2@mPDA-HCG nanoparticle-composite hydrogels. (B) SEM images of HCG (bars=80 μm) and Au/E2@mPDA-HCG (bars=50 μm) nanoparticle-composite hydrogels. (C) Pore size analysis of HCG and Au/E2@mPDA-HCG nanoparticle-composite hydrogels. (D) In vitro drug release (Black) and transdermal permeation (Red) of HCG and Au/E2@mPDA-HCG nanoparticle-composite hydrogels.

In vitro Anti-Photoaging Effect of Au/E2@mPDA-HCG Nanoparticle-Composite Hydrogel

Under UV irradiation, keratinocytes and other skin-related cells secrete a large number of pro-inflammatory cytokines, such as IL-6, which play a critical role in UV-induced skin inflammation. This leads to edema and erythema, compromises the integrity of the skin barrier, increases the expression of chemokines and other inflammatory molecules, and promotes the generation of ROS.³³ The sharp increase in ROS levels further exacerbates oxidative stress, leading to skin cell aging, while activating the release of matrix metalloproteinases (MMPs) in keratinocytes and fibroblasts. These enzymes degrade collagen and other extracellular matrix (ECM) proteins and inhibit collagen synthesis.^{34,35} Therefore, to investigate whether the Au/E2@mPDA-HCG nanoparticle-composite hydrogel provides protective effects against photoaging, this study used human keratinocytes (HaCaT) as an in vitro cell model. Various interventions were applied, and a series of experiments were conducted, including CCK-8 assays, SA-β-gal staining, fluorescence staining, MDA and SOD content determination, and Western blot analysis. These were systematically assessed to evaluate the effects of the hydrogel on cell viability, photoaging, oxidative stress, inflammation, and collagen synthesis.

Firstly, the CCK-8 assay was used to evaluate the effect of different concentrations of Au/E2@mPDA-HCG nanoparticle-composite hydrogel (5, 10, 15, 20, and 25 μg/mL) on HaCaT cell viability. The results showed (Figure 5A) that at a concentration of 25 μg/mL, the cell viability of HaCaT cells was still above 90%, indicating good biocompatibility. Further, the effects of different interventions on cell viability were examined. The results (Figure 5B) demonstrated that UVB irradiation significantly decreased HaCaT cell viability ($P < 0.001$), while E2 and Au/E2@mPDA-HCG treatments significantly enhanced cell viability ($P < 0.05$). Notably, the enhancement of

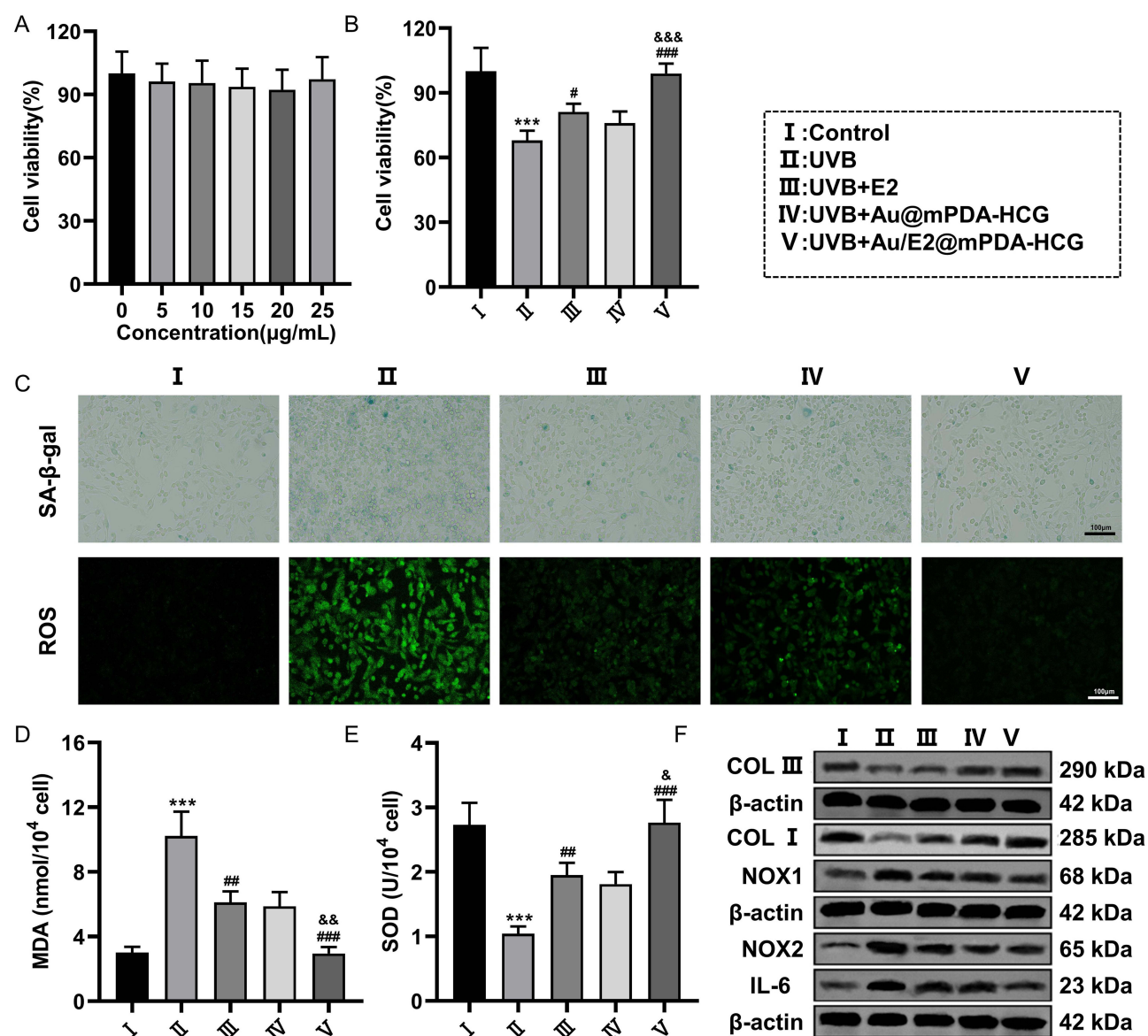


Figure 5 In vitro anti-photoaging effect of Au/E2@mPDA-HCG nanoparticle-composite hydrogel. (A) CCK-8 assay to detect the cytotoxicity of Au/E2@mPDA-HCG hydrogel. (B) CCK-8 assay to detect cell viability. (C) β-galactosidase staining (top, 200×, bars = 100 μm) to observe the degree of cell senescence and fluorescence staining (bottom, 200×, bars = 100 μm) to detect ROS levels in cells. (D) MDA level detection. (E) SOD level detection. (F) Western blot assay to detect the expression levels of COL III, COL I, NOX1, NOX2, and IL-6 in cells. Control: HaCaT cells with no intervention. UVB: HaCaT cells treated with UVB irradiation only. UVB+E2: HaCaT cells treated with UVB irradiation and E2 intervention. UVB+Au@mPDA-HCG: HaCaT cells treated with UVB irradiation and UVB+Au@mPDA-HCG intervention. UVB+Au/E2@mPDA-HCG: HaCaT cells treated with UVB irradiation and Au/E2@mPDA-HCG intervention. *** $P < 0.001$ vs Control, # $P < 0.05$ vs UVB, ### $P < 0.01$ vs UVB, #### $P < 0.001$ vs UVB, & $P < 0.05$ vs UVB+E2, && $P < 0.01$ vs UVB+E2, &&& $P < 0.001$ vs UVB+E2.

cell viability by Au/E2@mPDA-HCG was more pronounced compared to E2 ($P < 0.001$). In addition, SA-β-gal staining, fluorescence staining, and MDA and SOD content measurement results (Figure 5C–E) showed that UVB exposure increased the levels of SA-β-Gal, ROS, and MDA in HaCaT cells, while decreasing SOD levels. Both E2 and Au/E2@mPDA-HCG treatments significantly ameliorated these effects, with Au/E2@mPDA-HCG showing better efficacy than E2. Western blot analysis (Figure 5F) further confirmed these findings. After UVB irradiation, the expression levels of inflammation-related proteins (IL-6) and oxidative stress-related proteins (NOX1, NOX2) were increased, while collagen expression (COL I, COL III) decreased. However, after treatment with E2 and Au/E2@mPDA-HCG, the abnormal expression of these proteins was improved, and the effect of

Au/E2@mPDA-HCG was significantly better than that of E2. These results suggest that both E2 and Au/E2@mPDA-HCG have anti-photoaging effects on skin, which may involve alleviating oxidative stress, cell senescence, and inflammation.

Furthermore, compared to free E2, the Au/E2@mPDA-HCG nanoparticle-composite hydrogel exhibited a more pronounced anti-photoaging effect on the skin, which may be closely related to the characteristics of the Au@mPDA-HCG nanoparticle-composite hydrogel as a delivery vehicle. Studies have shown that mPDA NPs contain a high number of phenolic groups, which possess strong ROS-scavenging abilities.⁴⁴ As ROS levels decrease, the expression of pro-inflammatory cytokines is also reduced.⁴⁵ Additionally, HA has hygroscopic properties, and its secondary structure contains hydrophobic patch domains that can facilitate the penetration of the stratum corneum. Furthermore, the HA receptors on epidermal keratinocytes and dermal fibroblasts also assist in the transdermal delivery of HA to deeper tissues.⁴⁶ Taken together, these findings suggest that Au/E2@mPDA-HCG nanoparticle-composite hydrogels can effectively enhance the anti-photoaging effects of E2 on the skin.

In vivo Anti-Photoaging Effect of Au/E2@mPDA-HCG Nanoparticle-Composite Hydrogel

Based on the previous research findings, this study has demonstrated that estrogen deficiency exacerbates photoaging, while the Au/E2@mPDA-HCG nanoparticle-composite hydrogel exhibits significant in vitro anti-photoaging effects. Therefore, to further investigate the protective effect of the Au/E2@mPDA-HCG nanoparticle-composite hydrogel in vivo on photoaging aggravated by estrogen deficiency, we established an OVX mouse model and applied different interventions. Experimental results (Figure 6A) showed that, compared to the UVB+OVX group, the UVB+OVX+E2 and UVB+OVX+Au/E2@mPDA-HCG groups exhibited improved skin damage, with the UVB+OVX+Au/E2@mPDA-HCG group showing the best improvement. HE and Masson staining results (Figure 6B) further revealed that, compared to the UVB+OVX group, the UVB+OVX+E2 and UVB+OVX+Au/E2@mPDA-HCG groups had reduced epidermal thickness, increased dermal thickness, and enhanced collagen content, with Au/E2@mPDA-HCG showing better effects than UVB+OVX+E2. E2 content measurement results (Figure 7A) showed that, compared to the UVB+OVX group, the UVB+OVX+E2 and UVB+OVX+Au/E2@mPDA-HCG groups had significantly elevated serum E2 levels ($P<0.001$), with the UVB+OVX+Au/E2@mPDA-HCG group showing a more significant increase ($P<0.001$). Additionally, DHE staining, MDA, and SOD level measurements (Figures 6C, 7B and C) showed that, compared to the UVB+OVX group, the UVB+OVX+E2 and UVB+OVX+Au/E2@mPDA-HCG groups had significantly reduced ROS and MDA levels in the skin, along with significantly increased SOD levels. Notably, the UVB+OVX+Au/E2@mPDA-HCG group exhibited a more significant improvement in these indicators than the E2 group. Western blot analysis further confirmed these findings (Figure 7D), showing that, compared to the UVB+OVX group, the UVB+OVX+E2 and UVB+OVX+Au/E2@mPDA-HCG groups had decreased levels of inflammatory-related proteins (IL-6) and oxidative stress-related proteins (NOX1, NOX2) in the skin tissue, and increased levels of collagen (COL I, COL III). The UVB+OVX+Au/E2@mPDA-HCG group exhibited more significant regulation of these protein expressions. In conclusion, consistent with the in vitro results, the Au/E2@mPDA-HCG nanoparticle-composite hydrogel in vivo can significantly elevate E2 levels, alleviate oxidative stress and inflammation, and promote collagen synthesis, thereby enhancing the anti-photoaging effects of E2.

Conclusion

Estrogen is considered a potential therapeutic agent for skin photoaging, although its role and underlying mechanisms in UVB-induced photoaging remain unclear. Our findings demonstrate that estrogen deficiency accelerates skin photoaging by exacerbating oxidative stress and reducing collagen synthesis. In addition, given the clinical limitations of estrogen, such as low bioavailability and potential adverse effects, we developed an Au/E2@mPDA-HCG nanocomposite hydrogel

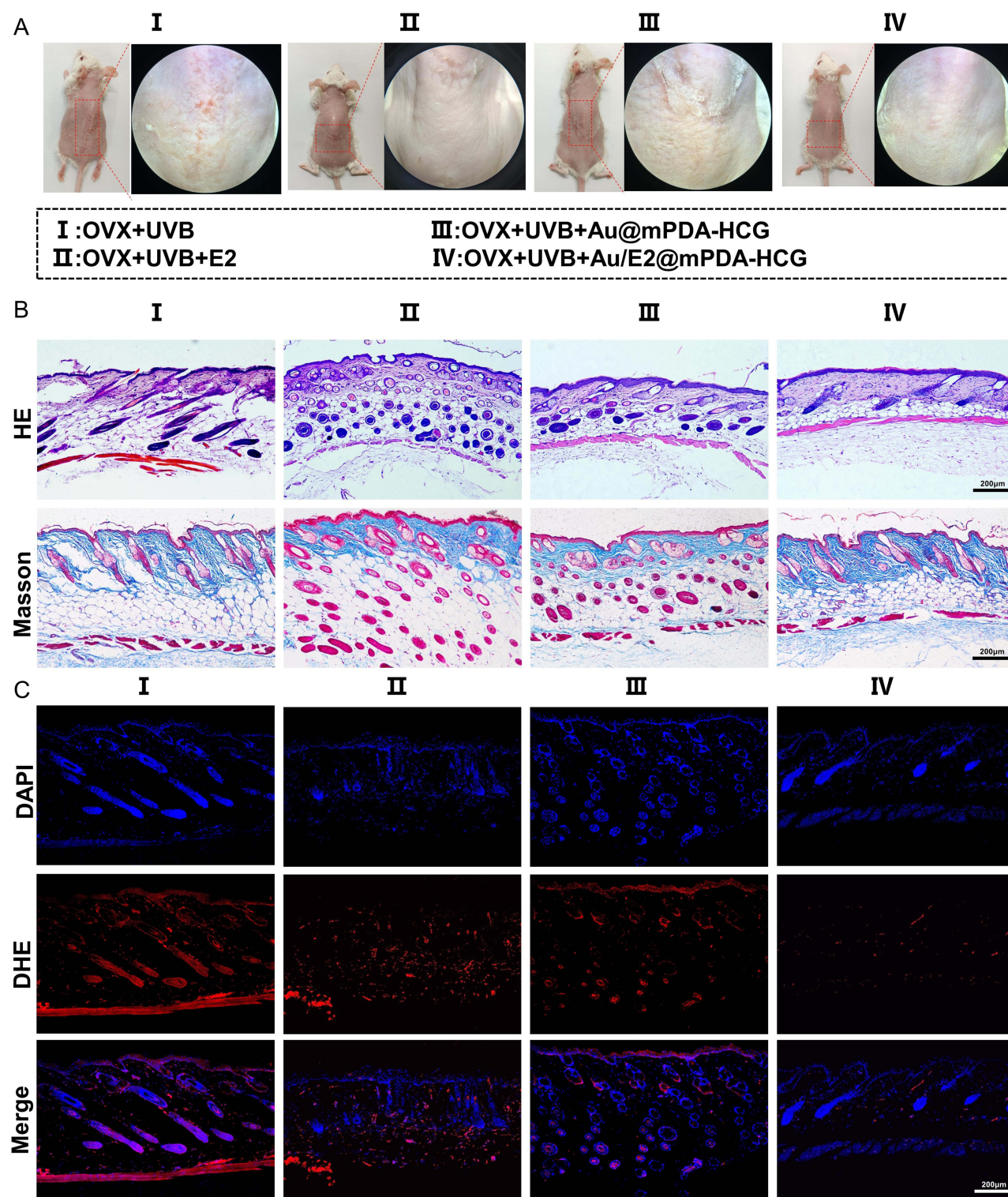


Figure 6 In vivo anti-photoaging effect of Au/E2@mPDA-HCG nanoparticle-composite hydrogel. **(A)** Morphological changes in mouse skin after different interventions. **(B)** HE staining (100 \times , n=3, top) and Masson staining (100 \times , n=3, bottom), bars=200 μ m. **(C)** DHE staining to detect ROS levels in mouse skin (100 \times , n=3), bars=200 μ m. UVB +OVX, mice subjected to UVB irradiation and OVX surgery. UVB+OVX+E2, mice subjected to UVB irradiation, OVX surgery, and E2 treatment. UVB+OVX+Au/E2@mPDA-HCG, mice subjected to UVB irradiation, OVX surgery, and Au/E2@mPDA-HCG treatment.

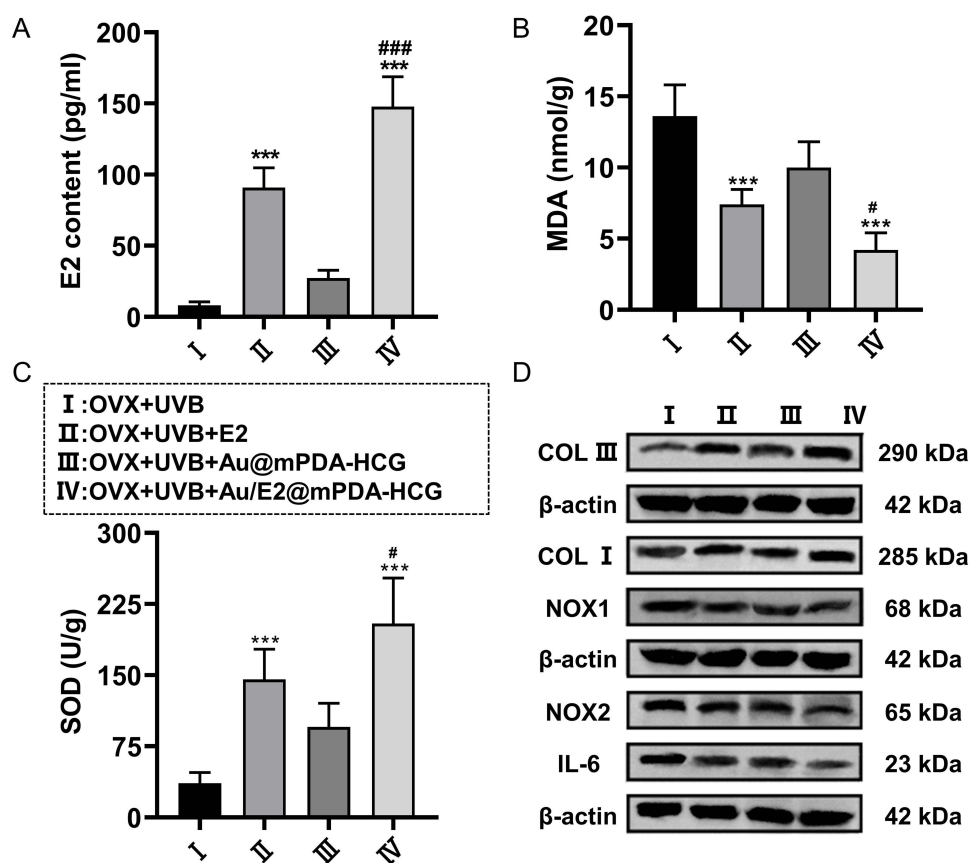


Figure 7 In vivo anti-oxidative stress and inflammation response, and enhancement of collagen generation by Au/E2@mPDA-HCG nanoparticle-composite hydrogel. **(A)** E2 content detection (n=6). **(B)** MDA content detection (n=6). **(C)** SOD content detection (n=6). **(D)** Western blot detection of COL III, COL I, NOX1, NOX2, and IL-6 expression levels in skin (n=3). UVB+OVX, mice subjected to UVB irradiation and OVX surgery. UVB+OVX+E2, mice subjected to UVB irradiation, OVX surgery, and E2 treatment. UVB+OVX+Au/E2@mPDA-HCG, mice subjected to UVB irradiation, OVX surgery, and Au/E2@mPDA-HCG treatment. UVB+OVX+Au/E2@mPDA-HCG, mice subjected to UVB irradiation, OVX surgery, and Au/E2@mPDA-HCG treatment. *** $P < 0.001$ vs UVB+OVX, # $P < 0.05$ vs UVB+OVX+E2, ### $P < 0.001$ vs UVB+OVX+E2.

for estrogen delivery. This nanocomposite hydrogel exhibited excellent stability and biocompatibility, and both in vitro and in vivo experiments revealed that it exerts superior anti-photoaging effects compared to E2 alone. Specifically, the hydrogel effectively mitigated oxidative stress and inflammatory responses while promoting collagen synthesis, thereby improving the features of skin photoaging. These enhanced effects may be attributed to the abundant phenolic groups in the mPDA structure, which possess strong reactive oxygen species scavenging abilities, as well as to the HA receptors on keratinocytes and dermal fibroblasts that may facilitate skin penetration and further enhance the anti-photoaging effects of estrogen. In summary, our study provides new insights into the role of estrogen in skin photoaging and demonstrates the significant potential of the Au/E2@mPDA-HCG nanocomposite hydrogel for the treatment of UVB-induced skin photoaging. Future studies will focus on further optimizing the nanocarrier system, increasing the sample size, and validating its safety and efficacy in larger-scale animal experiments and clinical trials, while exploring its potential applications in other skin disorders.

Abbreviations

E2, 17 β -estradiol; Au, gold; mPDA, mesoporous polydopamine; HA, hyaluronic acid; CMCS, carboxymethyl chitosan; UV, ultraviolet; UVB, ultraviolet B; ROS, reactive oxygen species; E1, estrone; IGF-1, insulin-like growth factor 1; NPs, nanoparticles; MDA, malondialdehyde; SOD, superoxide dismutase; CAT, catalase; GPx, glutathione peroxidase; SASP, senescence-associated secretory phenotype; MMP, metalloproteinase; DHE, dihydroethidium; ECM, extracellular matrix; HaCaT, human keratinocytes cells; OVX, ovariectomy; ELISA, Enzyme-linked immunosorbent assay; OD, optical

density; FTIR, Fourier-transform infrared spectroscopy; XRD, X-ray powder diffraction; DLS, dynamic light scattering; SA- β -gal, Senescence-associated β -Galactosidase; PVDF, Polyvinylidene Fluoride.

Data Sharing Statement

Data will be made available on request.

Funding

The project was funded by Wenzhou Municipal Science and Technology Bureau (Y2023461).

Disclosure

The authors report no declarations of interest.

References

1. Zhang H, Xiao X, Wang L. et al. Human adipose and umbilical cord mesenchymal stem cell-derived extracellular vesicles mitigate photoaging via TIMP1/Notch1. *Signal Transduct Target Ther.* 2024;9(1):294. doi:10.1038/s41392-024-01993-z
2. Yan L, Liu Z, Zeng Y, et al. Nanowire-based squalene oleogel repairs skin photoaging. *J Nanobiotechnology.* 2025;23(1):142. doi:10.1186/s12951-025-03233-0
3. Yao K, Peng Y, Tang Q, Liu K, Peng C. Human serum albumin/selenium complex nanoparticles protect the skin from photoaging injury. *Int J Nanomed.* 2024;19:9161–9174. doi:10.2147/IJN.S446090
4. Guo X, He L, Sun J, et al. Exploring the potential of anthocyanins for repairing photoaged skin. a comprehensive review. *Foods.* 2024;13. doi:10.3390/foods13213506.
5. Martinez-Alvarado Y, Amezcua-Galvez E, Davila-Rodriguez J, et al. Pirfenidone protects from UVB-induced photodamage in hairless mice. *Molecules.* 2023;29(1):28. doi:10.3390/molecules28072929
6. Dusabimana T, Karekezi J, Nugroho TA, et al. Oyster hydrolysate ameliorates UVB-induced skin dehydration and barrier dysfunction. *Life Sci.* 2024;358:123149. doi:10.1016/j.lfs.2024.123149
7. Chen W, Deng Q, Deng B, et al. Comprehensive analysis of hibisci mutabilis folium extract's mechanisms in alleviating UV-induced skin photoaging through enhanced network pharmacology and experimental validation. *Front Pharmacol.* 2024;15:1431391. doi:10.3389/fphar.2024.1431391
8. Chang KC, Wang Y, Oh IG, et al. Estrogen receptor beta is a novel therapeutic target for photoaging. *mol Pharmacol.* 2010;77(5):744–750. doi:10.1124/mol.109.062877
9. Wilkinson HN, Hardman MJ. A role for estrogen in skin ageing and dermal biomechanics. *Mech Ageing Dev.* 2021;197:111513. doi:10.1016/j.mad.2021.111513
10. Liu T, Li N, Yan YQ, et al. Recent advances in the anti-aging effects of phytoestrogens on collagen, water content, and oxidative stress. *Phytother Res.* 2020;34(3):435–447. doi:10.1002/ptr.6538
11. Weissberger AJ, Ho KK, Lazarus L. Contrasting effects of oral and transdermal routes of estrogen replacement therapy on 24-hour growth hormone (GH) secretion, insulin-like growth factor I, and GH-binding protein in postmenopausal women. *J Clin Endocrinol Metab.* 1991;72(2):374–381. doi:10.1210/jcem-72-2-374
12. Hong C, Song D, Lee DK, et al. Reducing posttreatment relapse in cleft lip palatal expansion using an injectable estrogen-nanodiamond hydrogel. *Proc Natl Acad Sci U S A.* 2017;114(35):E7218–E7225. doi:10.1073/pnas.1704027114
13. Zhou F, He Y, Zhang M, et al. Polydopamine(PDA)-coated diselenide-bridged mesoporous silica-based nanoplatfor for neuroprotection by reducing oxidative stress and targeting neuroinflammation in intracerebral hemorrhage. *J Nanobiotechnology.* 2024;22(1):731. doi:10.1186/s12951-024-03023-0
14. Chen Y, Feng X. Gold nanoparticles for skin drug delivery. *Int J Pharm.* 2022;625:122122. doi:10.1016/j.ijpharm.2022.122122
15. Dhandapani S, Wang R, Cheol hwang K, Kim H, Kim Y-J. Enhanced skin anti-inflammatory and moisturizing action of gold nanoparticles produced utilizing Diospyros kaki fruit extracts. *Arabian J. Chem.* 2023;16(4):104551. doi:10.1016/j.arabjc.2023.104551
16. Mohamed T, Matou-Nasri S, Farooq A, Whitehead D, Azzawi M. Polyvinylpyrrolidone-coated gold nanoparticles inhibit endothelial cell viability, proliferation, and ERK1/2 phosphorylation and reduce the magnitude of endothelial-independent dilator responses in isolated aortic vessels. *Int J Nanomed.* 2017;12:8813–8830. doi:10.2147/IJN.S133093
17. Georgeous J, AlSawaftah N, Abuwatfa WH, Hussein GA. Review of gold nanoparticles: synthesis, properties, shapes, cellular uptake, targeting, release mechanisms and applications in drug delivery and therapy. *Pharmaceutics.* 2024;16(10):1332. doi:10.3390/pharmaceutics16101332
18. Ibrahim B, Akere TH, Chakraborty S, Valsami-Jones E, Ali-Boucetta H. Functionalized gold nanoparticles suppress the proliferation of human lung alveolar adenocarcinoma cells by deubiquitinating enzymes inhibition. *ACS Omega.* 2023;8(43):40622–40638. doi:10.1021/acsomega.3c05452
19. Huang X, Chen L, Lin Y, et al. Tumor targeting and penetrating biomimetic mesoporous polydopamine nanoparticles facilitate photothermal killing and autophagy blocking for synergistic tumor ablation. *Acta Biomater.* 2021;136:456–472. doi:10.1016/j.actbio.2021.09.030
20. Liu Y, Wang C, Liu S, et al. Mesoporous polydopamine nanotherapeutics for MRI-guided cancer photothermal and anti-inflammatory therapy. *Int J Nanomed.* 2024;19:10819–10837. doi:10.2147/IJN.S467419
21. Zhou Y, Xu B, Zhou P, et al. Gold@mesoporous polydopamine nanoparticles modified self-healing hydrogel for sport-injuring therapy. *Int J Biol Macromol.* 2023;253:127441. doi:10.1016/j.ijbiomac.2023.127441
22. Liu C, Xia Y, Li Y, et al. Ligustrazine as an extract from medicinal and edible plant chuanxiong encapsulated in liposome-hydrogel exerting antioxidant effect on preventing skin photoaging. *Polymers (Basel).* 2022;14(21):4778. doi:10.3390/polym14214778

23. de Oliveira MM, Nakamura CV, Auzely-Velty R. Boronate-ester crosslinked hyaluronic acid hydrogels for dihydrocaffeic acid delivery and fibroblasts protection against UVB irradiation. *Carbohydr Polym.* **2020**;247:116845. doi:10.1016/j.carbpol.2020.116845
24. Li S, Sun J, Yang J, et al. Gelatin methacryloyl (GelMA) loaded with concentrated hypoxic pretreated adipose-derived mesenchymal stem cells(ADSCs) conditioned medium promotes wound healing and vascular regeneration in aged skin. *Biomater Res.* **2023**;27(1):11. doi:10.1186/s40824-023-00352-3
25. Wang HH, Yin HL, Yin WW, Song YL, Chen H. Cu(II)-based complex loaded with drug paclitaxel hydrogels against thyroid cancer and optimizing novel derivatives. *Sci Rep.* **2024**;14(1):13050. doi:10.1038/s41598-024-63940-w
26. Wang Z, Yuan J, Xu Y, et al. Olea europaea leaf exosome-like nanovesicles encapsulated in a hyaluronic acid / tannic acid hydrogel dressing with dual “defense-repair” effects for treating skin photoaging. *Mater Today Bio.* **2024**;26:101103. doi:10.1016/j.mtbio.2024.101103
27. Yue Y, Liu Y, Lin Y, et al. A carboxymethyl chitosan/oxidized hyaluronic acid composite hydrogel dressing loading with stem cell exosome for chronic inflammation wounds healing. *Int J Biol Macromol.* **2024**;257:128534. doi:10.1016/j.ijbiomac.2023.128534
28. Zhang F, Zhang S, Lin R, et al. Injectable multifunctional carboxymethyl chitosan/hyaluronic acid hydrogel for drug delivery systems. *Int J Biol Macromol.* **2023**;249:125801. doi:10.1016/j.ijbiomac.2023.125801
29. Peng YS, Han K, Zhao JX, Song WC, Dai SQ. A new dy(III) complex: fluorescence performances, loading with resveratrol-hydrogels against skin aging and molecular docking. *J Fluoresc.* **2024**. doi: 10.1007/s10895-024-03683-z.
30. Rock K, Meusch M, Fuchs N, et al. Estradiol protects dermal hyaluronan/versican matrix during photoaging by release of epidermal growth factor from keratinocytes. *J Biol Chem.* **2012**;287(24):20056–20069. doi:10.1074/jbc.M112.353151
31. Liu H-M, Cheng M-Y, Xun M-H, et al. Possible mechanisms of oxidative stress-induced skin cellular senescence, inflammation, and cancer and the therapeutic potential of plant polyphenols. *Int J Mol Sci.* **2023**;24(4):3755. doi:10.3390/ijms24043755
32. Han J, Wu T, Jin J, et al. Exosome-like nanovesicles derived from *Phellinus linteus* inhibit Mical2 expression through cross-kingdom regulation and inhibit ultraviolet-induced skin aging. *J Nanobiotechnology.* **2022**;20(1):455. doi:10.1186/s12951-022-01657-6
33. Truong V-L, Rarison RH, Jeong W-S. Protective effects of orange sweet pepper juices prepared by high-speed blender and low-speed masticating juicer against UVB-induced skin damage in SKH-1 hairless mice. *Molecules.* **2022**;27(19):6394. doi:10.3390/molecules27196394
34. Fu Y, Li C, Wang Q, et al. The protective effect of collagen peptides from bigeye tuna (*Thunnus obesus*) skin and bone to attenuate UVB-induced photoaging via MAPK and TGF- β signaling pathways. *Journal of Functional Foods.* **2022**;93:105101. doi:10.1016/j.jff.2022.105101
35. Zhang R, Wei Y, Zhang J, et al. Protection effects of rice protein hydrolysate on UVB-irradiated photodamage in Hartley Guinea pigs skin and human skin fibroblasts. *Journal of Functional Foods.* **2021**;82:104504. doi:10.1016/j.jff.2021.104504
36. Zheng S, Deng R, Huang G, Ou Z, Shen Z. Screening the active ingredients of plants via molecular docking technology and evaluating their ability to reduce skin photoaging. *Biogerontology.* **2024**;25(6):1115–1143. doi:10.1007/s10522-024-10125-7
37. Jiang X, Yu X, Hu S, et al. Effects of E2 on the IDO1-mediated metabolic KYN pathway in OVX female mice. *J Cell mol Med.* **2024**;28(20):e70179. doi:10.1111/jcmm.70179
38. Wang T, Wang Y, Zhang Y, et al. Drug-loaded mesoporous polydopamine nanoparticles in chitosan hydrogels enable myocardial infarction repair through ROS scavenging and inhibition of apoptosis. *ACS Appl Mater Interfaces.* **2024**;16(45):61551–61564. doi:10.1021/acsami.4c08155
39. Ma X, Cui Y, Zhang M, Lyu Q, Zhao J. A multifunctional nanodrug co-delivering VEGF-siRNA and dexamethasone for synergistic therapy in ocular neovascular diseases. *Int J Nanomed.* **2024**;19:12369–12387. doi:10.2147/IJN.S492363
40. Yu Z, Gan Z, Wu W, et al. Photothermal-triggered extracellular matrix clearance and dendritic cell maturation for enhanced osteosarcoma immunotherapy. *ACS Appl Mater Interfaces.* **2024**. doi:10.1021/acsami.4c12532
41. Nakka NMR, Rachamala HK, Angom RS, et al. Dual drug-loaded tumor-targeted polymeric nanoparticles for enhancing therapeutic response in pancreatic ductal adenocarcinoma. *Mater Today Bio.* **2024**;28:101199. doi:10.1016/j.mtbio.2024.101199
42. Zhang X, Xu B, Ni J, Xiang Y, He Z. Combined chemo- and photothermal therapies of non-small cell lung cancer using polydopamine/au hollow nanospheres loaded with doxorubicin. *Int J Nanomed.* **2024**;19:9597–9612. doi:10.2147/IJN.S473137
43. Kondiah PPD, Rants'o TA, Mdanda S, Mohlomi LM, Choonara YE. A poly (caprolactone)-cellulose nanocomposite hydrogel for transdermal delivery of hydrocortisone in treating psoriasis vulgaris. *Polymers (Basel).* **2022**;14(13). doi:10.3390/polym14132633
44. Fu Y, Yang L, Zhang J, et al. Polydopamine antibacterial materials. *Mater Horiz.* **2021**;8(6):1618–1633. doi:10.1039/d0mh01985b
45. Deng QS, Gao Y, Rui BY, et al. Double-network hydrogel enhanced by SS31-loaded mesoporous polydopamine nanoparticles: symphonic collaboration of near-infrared photothermal antibacterial effect and mitochondrial maintenance for full-thickness wound healing in diabetes mellitus. *Bioact Mater.* **2023**;27:409–428. doi:10.1016/j.bioactmat.2023.04.004
46. Han HH, Kim SJ, Kim J, et al. Bimetallic hyaluronate-modified Au@Pt nanoparticles for noninvasive photoacoustic imaging and photothermal therapy of skin cancer. *ACS Appl Mater Interfaces.* **2023**;15(9):11609–11620. doi:10.1021/acsami.3c01858